ACS OMEGA

Open Access

http://pubs.acs.org/journal/acsodf

Article

Metal–Plastic Hybrid Additive Manufacturing to Realize Small-Scale Self-Propelled Catalytic Engines

Adhikarige Taniya Kaushalya Perera, Kewei Song, Xiangyi Meng, Wei Yang Wan, Shinjiro Umezu,* and Hirotaka Sato*

Cite This: *ACS Omega* 2024, 9, 283−293

Read Online

ACCESS | Metrics & More | Article Recommendations | Supporting Information

ABSTRACT: Microengines driven by catalytic decomposition of a fuel have been an interesting research area recently due to their diverse applications, such as environmental monitoring and drug delivery. Literature reports a number of studies on this topic where researchers have made various attempts to manufacture such microengines. Some such methods are deposition of catalytic metal layers on sacrificial photoresists, electrochemical deposition of metal layers on polymeric structures, or 3D printing of structures followed by multi-step loading of structures with catalysts. These methods, even though proven to be effective, are tedious, time-consuming, and expensive. To address these issues, herein we report a 3D printing technique to realize microengines in a simple, rapid, and inexpensive single-step process. The printing of various shapes of microengines is achieved using digital light processing printing of a catalyst resin, where Pd(II) acts as a catalyst resin. The proposed integrated molding process can achieve cost-effective preparation of high-efficiency microengines. We demonstrate the locomotion of these microengines in 30% (w/w) H_2O_2 through the decomposition of H_2O_2 to generate oxygen to facilitate the self-propelled locomotion. The study characterizes the microengine based on several factors, such as the role of H_2O_2, Pd, shape, and design of the microengine, to get a full picture of the self-locomotion of microengines. The study shows that the developed method is feasible to manufacture microengines in a simple, rapid, and inexpensive manner to be suitable for numerous applications such as environmental monitoring, remediation, drug delivery, diagnosis, etc., through the modification of the catalyst resin and fuel, as desired.

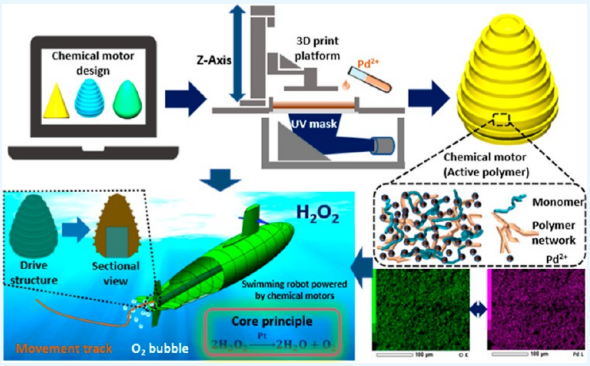

1. INTRODUCTION

The locomotion of synthetic microengines has been discussed by researchers over the last two decades pertaining to their applications in numerous fields[1−6] such as environmental monitoring,[7] drug delivery,[8] microsystem assembly,[9] etc. These microengines realize their motion through various methods, and some of the various available microengines are self-diffusiophoretic swimmers, bimetallic nanorods, catalytically activated microengines, and nature-inspired microengines driven by the rotation or wave movement of flagella.[10−12] Among these, catalytically activated motors, or microengines, that convert the energy of a chemical reaction into a driving force for the locomotion of the engine have attracted the attention of many over the past two decades. Such microengines utilize a catalyst to initiate and trigger a decomposition reaction of the fuel, which in turn results in a bubbling of oxygen or hydrogen that creates a bubbling propulsion to drive the motor.[1,2,6,10,13−15] One such early study that inspired the researchers is Whiteside's study of the self-propulsion of a plate by oxygen bubbles created through Pt-catalytic decomposition of hydrogen peroxide (H_2O_2).[16] Other than Pt,[2,6,10,17] researchers have also been using other catalytic materials such as Ag and MnO_2 with H_2O_2 as fuel for the decomposition reaction.[18] Another option for fuel is acid with Zn as the catalyst, and the propulsion would be facilitated by hydrogen created through the decomposition of acid.[19,20] Water can also be utilized as a fuel with the Al−Ga alloy, where Al acts as the catalyst to reduce water to hydrogen and Ga acts to hinder the passivation of Al due to the formation of $Al(OH)_3$.[21] Mg has also been utilized as the catalyst in the presence of water as a media or fuel by several researchers.[22−24] However, the Pt−H_2O_2 system can be identified as the most studied system for catalytic locomotion in microengines. The decomposition reaction is as follows.

$$2H_2O_2 \xrightarrow{Pt} 2H_2O + O_2 \quad (1)$$

Received: July 19, 2023
Revised: November 13, 2023
Accepted: November 14, 2023
Published: December 26, 2023

Over the years, reported attempts at manufacturing microengines have been achieved mostly through the deposition of multimetal layers onto sacrificial photoresist layers and electrochemical synthesis onto polymeric structures, which are tedious and time-consuming processes.[1,2,6,10] 3D printing has also been reported by Zhu et al. to fabricate a microfish with a Pt catalyst and Fe_3O_4 as magnetic particles.[25] Here, the particle loading on the fish is carried out in a multi-step process which requires the replacement of polymeric solutions at each stage. Magnetic particle addition is practiced by many researchers in microengine locomotion as the guiding method for the movement of the microengine. This magnetic layer is also achieved through the methods discussed above.[1,2,6,10]

Still, going through the literature, we find that no attempt is made at the simple, rapid, and inexpensive fabrication of microengines in a single step-process. In such a scenario, 3D printing or additive manufacturing stands as a promising method to develop such processes to realize microengines in a simple and rapid manner. 3D printing stands among other methods due to its capability of manufacturing sophisticated 3D structures with fine details in a vast range of materials.[26,27] Further, the technology offers printing with modified materials to enhance the properties of the printed structures.[28−32]

Herein, we report a simple and rapid method to manufacture microengines with a modified resin in a single step. Previously, our group has reported 3D printing of complex 3D structures with a catalyst resin, where resins are embedded with catalyst particles prior to the printing to facilitate the electroless deposition (ELD) of desired metals selectively or nonselectively on these 3D structures.[28−30] Here, we adopt the modification of resin to print the microengine in a single-step process through a customized commercial digital light processing (DLP) printer. Resin is modified by adding a metal salt solution to the catalyst of interest. The resin and metal salt solution are thoroughly mixed prior to printing. Differing from our previous studies, here we skip the ELD of a catalytic metal layer to facilitate the decomposition of our fuel of choice, which is H_2O_2. Instead, we directly add the catalyst in its metal salt form to the resin and later reduce the ionic particles into elemental particles by chemical reduction of the structure.

Also, to address the cost effectiveness of the process, instead of precious metals such as Pt, we use Pd^{2+}-containing polymers, which reduce development costs compared with the conventional process. Pd possesses the ability to replace Pt in terms of participation in similar kinds of reactions, even though the activities are slightly lower than Pt.[33−36] During the development of our method, we use $PdCl_2$ as the catalytic precursor, and the concentration is kept at a highest of 700 ppm.[36] Since the metal salt is used instead of pure metal at given concentrations and a small volume of catalyst resin is required for the printing of small-scale microengines, the cost incurred for the process remains in a lower range, which is closer to a few cents of USD. The decomposition reaction remains the same except for the catalyst participating in the reaction, as follows:

$$2H_2O_2 \xrightarrow{Pd} 2H_2O+O_2 \quad (2)$$

During the current study, our core purpose is to explore new strategies for catalysis based on 3D structures fabricated by active polymers and to fabricate structurally controllable 3D-printed chemical motors based on this principle. Hence, we do not address the controlled locomotion of microengines via magnetic manipulation within the current scope of this study. Here, we study several designs based on the cone shape, which is chosen inspired by the microswimmer studies reported,[37−39] manufactured on a smaller scale for their self-propelled locomotion in H_2O_2. Further, we characterize these microengines based on several factors, such as their shape, internal cavity size, catalyst concentration, and fuel conditions. The method is a simple, rapid, and inexpensive process to realize microengines in a single step. Cooperating with the developed multimaterial 3D printing technology, the function of the chemical motor for directional control can be further improved by optimizing the resin mixture. This reported method shows the feasibility of realizing microengines with further enhanced properties such as magnetic manipulation and also its suitability to be utilized in various fields such as environmental monitoring and remediation, drug delivery, and diagnostics through modifying the catalyst and resin, as required, to be used with a fuel of choice.

2. EXPERIMENTS

2.1. Materials and Apparatus. eSun poly(methyl mecrylate) (PMMA)-like photopolymer resin was purchased from Shenzhen Esun Industrial Co., Ltd. (Viscosity: 200 mPa·s, density: 1.05−1.15 g/cm^3). $PdCl_2$, NH_4Cl, sodium hydroxide (NaOH), sodium hypophosphite monohydrate ($NaH_2PO_2 \cdot H_2O$), and hydrogen peroxide (H_2O_2) were purchased from Sigma-Aldrich, Singapore. All the solutions were prepared using type II deionized water (DIW) from Merck Milli Q IX7005 where necessary, and H_2O_2 was used as purchased in most of the experimental studies.

A vortexer was used in the preparation of the catalyst solution, and the catalyst resin mixture was prepared by well mixing the catalyst solution and resin manually.

A commercial Anycubic Photon D2 DLP 3D Printer (Anycubic Shenzhen, China), which was customized to obtain improved resolution by adjusting the distance between the optical module of the DLP component and the mask receiving surface (optical window distance), was employed in printing the samples using catalyst resins of various catalyst loadings and geometries. However, the maximum print size is sacrificed during the printing process.

2.2. Preparation of Catalyst Resin for Printing. The presence of catalyst is required for the self-propelling action of the chemical motor. Similar to our previous study,[30] we infused the resin with a catalyst precursor to produce a catalyst resin for printing. Pd was chosen as the catalyst of interest, which is capable of reacting with H_2O_2 and initiating the self-propelling action. $PdCl_2$ was selected as the Pd source. Stock solutions of 7000 and 3500 ppm Pd(II) were prepared by adding $PdCl_2$ to 0.7 M NH_4Cl and mixing in the vortex mixer until fully dissolved. A similar concentration of NH_4Cl is used in all stock solutions to avoid differences in NH_4Cl concentration in the final resin mixture. As prepared, Pd(II) solution was mixed with the photopolymer resin in a ratio of 9:1 of resin to Pd(II) solution, respectively. The mixture was stirred manually at room temperature until a single phase was obtained to get the final, ready-to-print catalyst resin.

2.3. Printing of Micro 3D Structures. The customized DLP printer operates under a 405 nm UV-LED light source at a 12 V dc voltage. DLP uses a digital micromirror device which controls the light patterns via an optical system to guide the solidification to the realized desired structure.[40] The Anycubic 3D printer that is employed here consumes low power and generates minimal heat during operation. To realize the desired

https://doi.org/10.1021/acsomega.3c04949
ACS Omega 2024, 9, 283−293

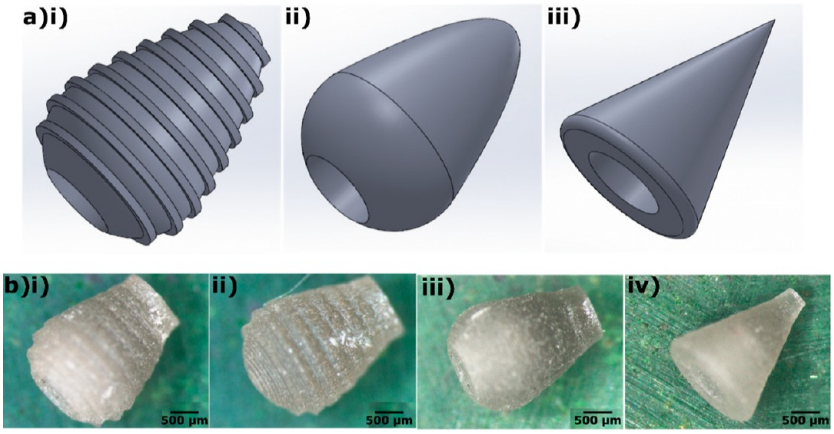

Figure 1. (a) Various designs modeled through SolidWorks to be tested as catalytic microengines: (i) Threaded ovoid with a cavity at the base, (ii) ovoid with a cavity at the base, and (iii) cone with a cavity at the base. (The diameter of the cavity was kept at 1 mm). (b) Printed structures observed under the optical microscope with a 2× magnification, (i) threaded ovoid with a larger cavity of 1 mm diameter, (ii) threaded ovoid with a smaller cavity of 0.3 mm diameter, (iii) ovoid with a cavity of 1 mm diameter, and (iv) cone with a cavity of 1 mm diameter. Apart from these designs, a threaded ovoid without a cavity at the base was also printed.

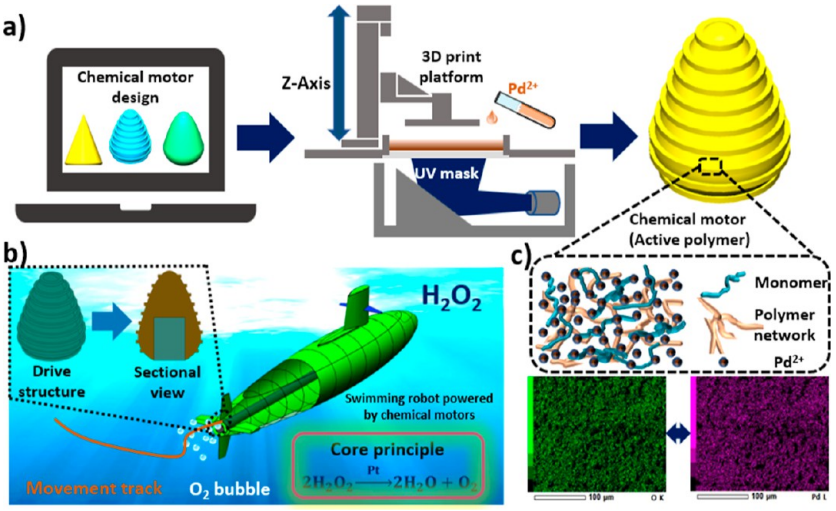

Figure 2. Schematic illustrating the fabrication process of catalytically active microengines with their locomotion principle. (a) Modeled designs, schematic of DLP printer, and printed design (from left to right). (b) Locomotion core principle of chemical motors or microengines. Inset shows the structure of a chemical motor with its sectional view. (c) Composition of catalyst resin is illustrated figuratively, cured by chemical bonding and cross-linking.

structures, the thickness of each layer was set to 0.05 mm, and the exposure time for the first 5 layers was set at 40 s for each layer, while for the rest of the layers it was set at 5 s. All the printing operations were conducted at room temperature. Once the printing is complete, the samples are cleaned with ethanol prior to and after the careful removal of the platform, rinsed with water, and air-dried under compressed air. Such prepared samples were cured using Anycubic wash and cure plus curing chamber (Anycubic, Shenzhen, China) for 40 min under UV light, further polymerization and cross-linking of polymers to enhance overall mechanical properties.

The structures were designed with Solid Works with dimensions of 2 mm base width ×3 mm height in the shapes of cone, ovoid, and threaded ovoid. The threads were added with the purpose of increasing the effective surface area for the catalytic reaction. The designs were created with or without a cavity at the base. The diameter of the cavity was kept at 1 or 0.2 mm. Also, the designed microengines were printed with catalyst resins with 700 and 350 ppm Pd concentrations and pure resin. The designs printed are illustrated as both design sketches in Figure 1a and printed devices in Figure 1b.

2.4. Pretreatment of Printed Microengines. The printed microengines were cured under UV light and stored in a cool, dry place; the design and the printed parts are shown in Figure 1. Prior to the study of their self-propelling action, it is required that the Pd precursors be reduced to elemental Pd to act as catalysts for the oxidation of H_2O_2. To achieve this, we first treat the printed structures with 0.2 M NaOH for 1 day. Treatment with NaOH leads to resin ring cleavage and enhancement of the presence of Pd precursors for catalytic activity. This process is explained in detail in our previous paper[30] Upon NaOH treatment, the printed structures are rinsed with DIW and then soaked in 4 M $NaH_2PO_2{\cdot}H_2O$ for 45 min to ensure the complete reduction of available Pd precursors to elemental Pd. The structures are again rinsed with DIW to remove excess $NaH_2PO_2{\cdot}H_2O$. The structures are now ready to be studied as self-propelled microengines.

https://doi.org/10.1021/acsomega.3c04949
ACS Omega 2024, 9, 283−293

2.5. Self-Propelled Locomotion of Printed Catalytic Engines. The treated and ready-to-study microengines were studied for their self-locomotive action in the presence of H_2O_2 in a Petri dish. The principle of their self-catalysis and thus movement is shown in Figure 2. Devices were tested one at a time by using 5 ML of H_2O_2 each time. As a control experiment, devices were tested in the presence of water to confirm that the movement in H_2O_2 is due to the catalytic oxidation of H_2O_2, which causes bubbling from the catalytic surface and creates a driving force for the movement of the device but not due to the buoyancy force or floating of the device. As another measure to ensure this, the volume of H_2O_2 is kept at 5 ML, which is roughly enough to fully dip the printed device when added to a Petri dish of 60 mm diameter. The movement is recorded for each device and each condition.

Later on, the average velocity of self-propelled movement is calculated for each device and condition that showed the movement by analyzing the videos through imageJ − an open-source software for image processing developed by the National Institute of Health, United States. Further analysis was carried out with MS Excel, and the Petri dish diameter was used as a reference for the calculations made.

3. RESULTS AND DISCUSSION

3.1. Preparation of Catalyst Resin Mixtures. During the present study, we chose a nonwatery-washable PMMA-like photopolymer resin as the resin of interest, considering its compatibility with the printer to provide structures with fine details and without cracks during the post-curing process. $PdCl_2$ is the catalytic precursor, and the solvent was chosen to be NH_4Cl despite the fact that the resin of choice is non water-washable. The choice was triggered by the ability of resin to make a single phase with water at a ratio of 9 parts resin: 1 part water upon well mixing. Following the results of our previous study, we used 0.7 M NH_4Cl to dissolve $PdCl_2$ and prepare stock solutions. Equation 3 illustrates the dissolving reaction of $PdCl_2$ in NH_4Cl.

$$PdCl_2 + 2NH_4Cl \rightarrow [Pd(NH_3)_2Cl_2] + 2HCl \quad (3)$$

Two types of catalyst resin mixtures with final Pd (II) concentrations of 700 and 350 ppm were prepared. The purpose was to study the effect of Pd concentration on the self-propelling movement of the catalytic microengine.

The prepared resin mixtures initially appeared light brown in color and became darker as time passed. The resin mixture gets blackened in around 3 to 4 h for the resin mixture with 700 ppm of Pd (II), while the resin mixture with 350 ppm of Pd (II) becomes dark brown. We believe the color change is due to the reactions between Pd (II) and resin, as we observed a darker color with the increase of Pd (II). Further we observed an improved catalytic action with an aged catalyst resin mixture when compared with a freshly prepared catalyst resin mixture. Hence, the color change could be attributed to the natural reactions between Pd (II) and resin, which lead to the reduction of Pd (II). However, the reactions are unclear, as the resin composition is unknown to us. Based on the observations and the defined hypothesis, the printing was carried out only 4 h after the preparation of the catalyst resin mixture.

The prepared catalyst resin mixture remained stable in its liquid state for more than 6 h providing the necessary time window to complete the printing of the required structures for multiple rounds. In addition to the catalyst resin mixtures, the microengine structure was also printed with pure resin to run a control experiment examining the effect of the Pd catalyst for the decomposition of H_2O_2. The darkening of the resin mixture over time for different catalyst resin mixtures is shown in Figure 3

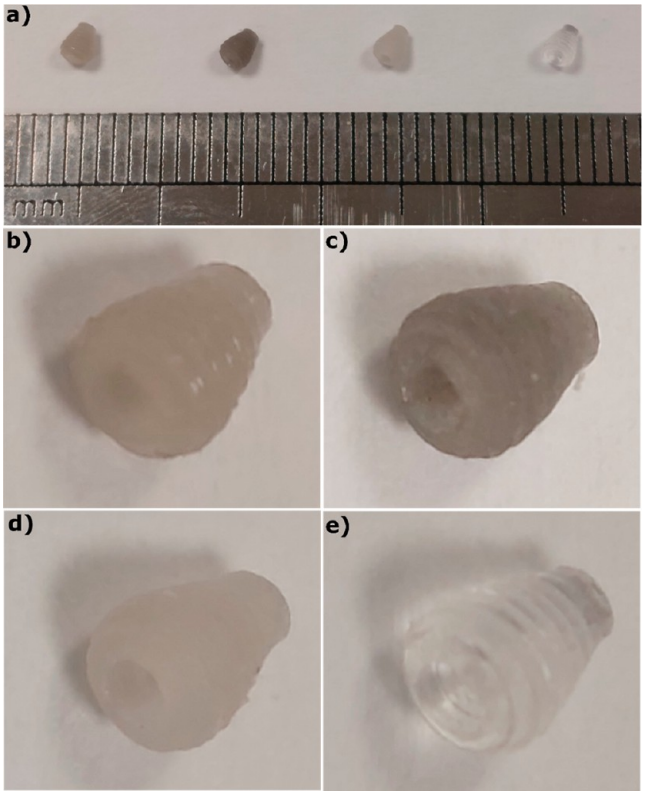

Figure 3. Darkening of the resin mixture over time along with the overall dimensions is shown with the printed microengines of different resin mixtures. (a) Overall dimensions of printed microengines (2 mm × 3 mm) are shown in comparison to a ruler. (b) Microengine printed with 700 ppm of Pd(II) concentration catalyst resin soon after mixing. (c) Microengine printed with 700 ppm of Pd(II) concentration catalyst resin 4 h after mixing. (d) Microengine printed with 350 ppm of Pd(II) concentration catalyst resin 4 h after mixing. (e) Microengine printed with pure resin.

along with a comparison of the overall dimensions of the printed structure. The printed structures were cured for 40 min under UV light. The post-curing step aids in keeping the structural stability of the printed designs without leading to the failure of the structure with time.

3.2. Self-Propelled Locomotion of Printed Catalytic Microengines. Herein, the cured samples are prepared under a variety of conditions for the comparative study of their self-propelled movement in H_2O_2. These variety of conditions include various designs of microengines, pretreatment of microengines, loading of Pd inside the structure, effect of cavity size at the base of the structure, concentration of H_2O_2, and effective surface area of the designed microengine.

3.2.1. Role of H_2O_2 for the Self-Propelled Locomotion of Printed Microengines. At the initial stage, it is essential to confirm that the locomotion is indeed driven by the decomposition of H_2O_2 by the presence of the catalyst in the structure but not by the buoyancy force created by the liquid. Here, H_2O_2 acts as fuel for the movement of catalytic microengines, where the decomposition of this solution leads to oxygen bubbling on the catalytic structure surface, leading to the movement of the catalytic microengine in the direction

https://doi.org/10.1021/acsomega.3c04949
ACS Omega 2024, 9, 283−293

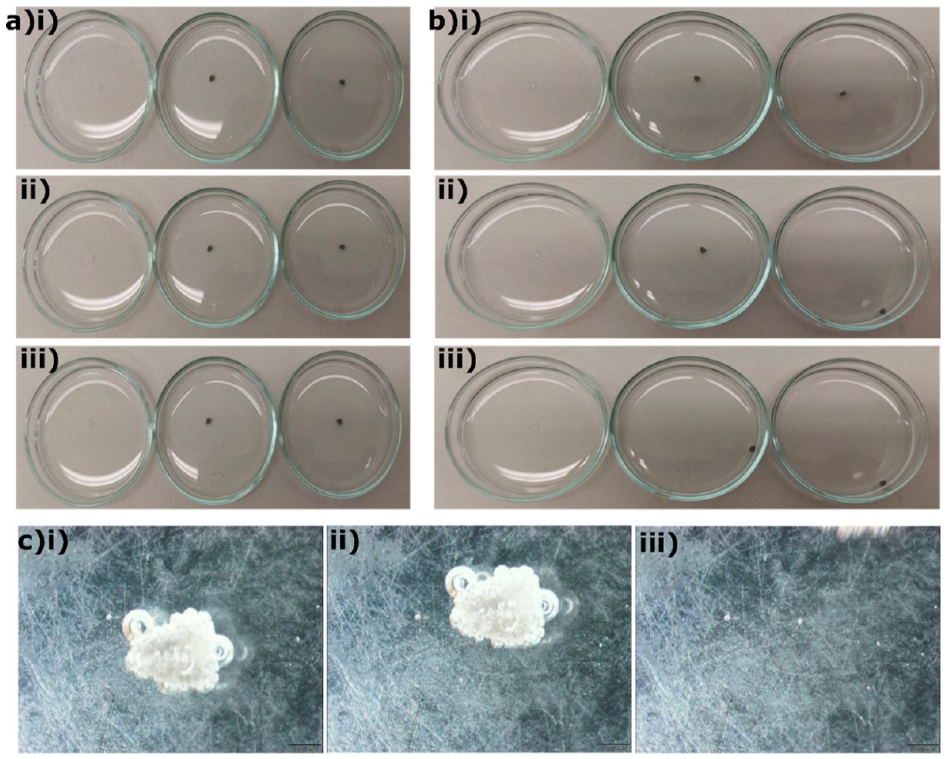

Figure 4. Time frames showing the movement of threaded ovoids with a larger cavity at the base in water and H_2O_2. (a) Movement in water (i) 0 s, (ii) 41 s, and (iii) 84 s. Time frames show that no movement is observed in water. (b) Movement in H_2O_2 (i) 0 s, (ii) 48 s (the threaded ovoid with elemental Pd reaches the edge of the Petri dish), and (iii) 121 s (the threaded ovoid with ionic Pd reaches the edge of the Petri dish). (c) Movement in H_2O_2 observed under a microscope at different times once the movement is initiated (i) 0, (ii) 1, and (iii) 2 s. The catalytic reaction of Pd with H_2O_2, creating oxygen bubbles, is visible here.

opposite to the bubbling based on Newton's third law. To minimize the buoyancy force, we have lowered the volume of H_2O_2 utilized in a single experiment to a limit of 5 ML, which is just enough to cover the base of a Petri dish with a 60 mm diameter and to fully dip any of the printed structures with ease. DIW is chosen as the media for the control experiment since it does not facilitate any catalytic reaction with Pd. This provides us with a controlled environment to study the effect of buoyancy on the microengine movement and confirm the theory of catalytic self-propelling action. Further, we employed microengine structures made of pure resin as well as catalyst resin with Pd in elemental form and in ionic form to further confirm the role of H_2O_2 to fuel the movement of microengines. Threaded ovoid with a larger cavity of 1 mm diameter at the base was chosen as the design of the microengine for these experiments.

When DIW is used as the medium, no movement was observed for any of the microengines that are fabricated with pure resin, catalyst resin where Pd is in ionic form, or catalyst resin with Pd in elemental form. The observation confirms that the effect of buoyancy is negligible on the movement of the microengine structure. The time frames of the study for DIW as media are provided in Figure 4a, while the same for H_2O_2 is provided in Figure 4b. The supplementary Videos S1 and S2 show the observations respective to Figure 4a,b. Upon confirming that it is not the buoyancy force that drives the locomotion of microengines, we moved on to study the locomotion of these structures in the presence of H_2O_2 as the fuel media. Herein, no movement was observed for the pure resin-fabricated microengine. However, a slowed-down movement was observed for the microengine comprised of Pd in ionic form. We believe that even though Pd is not reduced to its atomic form, a portion of it may have reached the atomic state during the aging of catalyst resin, and a portion of it might be present on the surface of the microengine. This might be the driving force behind the slowed locomotion of the microengine in this scenario. As for the microengine with Pd in elemental form, it showed a considerably rapid movement in the presence of H_2O_2 as the medium. This is due to the catalytic reaction of reduced Pd with H_2O_2, which leads to oxygen bubbling from the surface (inner and outer) of the microengine. The microengine moves in the opposite direction, to the side where most bubbles are formed. The calculated velocities upon analysis by ImageJ for the microengines with pure resin, catalyst resin with Pd in ionic form, and Pd in elemental form are 0 0.25 and 0.62 mm/s, respectively.

To further visualize the bubbling reaction in H_2O_2, these microengines were observed under a microscope for their movement. Here, it showed the catalytic reaction of Pd with H_2O_2 clearly with rigorous oxygen bubbling, and the movement was observed in the direction opposite to the most bubble-forming side of the microengine (supporting Video S6). The movement observed under the microscope is also shown in Figure 4c for the microengine with Pd in its elemental form.

3.2.2. Effect of Pretreatment of Structures with NaOH. Pretreatment conditions were treatment with 0.2 M NaOH for a day and reduction of Pd(II) into elemental Pd employing the reducing agent Sodium Hypophosphite at a concentration of 4 M for 45 min. The structures were treated with either of the solutions or both of the solutions, or they were not treated with any of the solutions for the control experiment. The control experiment with no treatment is discussed in Section 3.2.1, where it showed a slowed-down movement in H_2O_2.

https://doi.org/10.1021/acsomega.3c04949
ACS Omega 2024, 9, 283−293

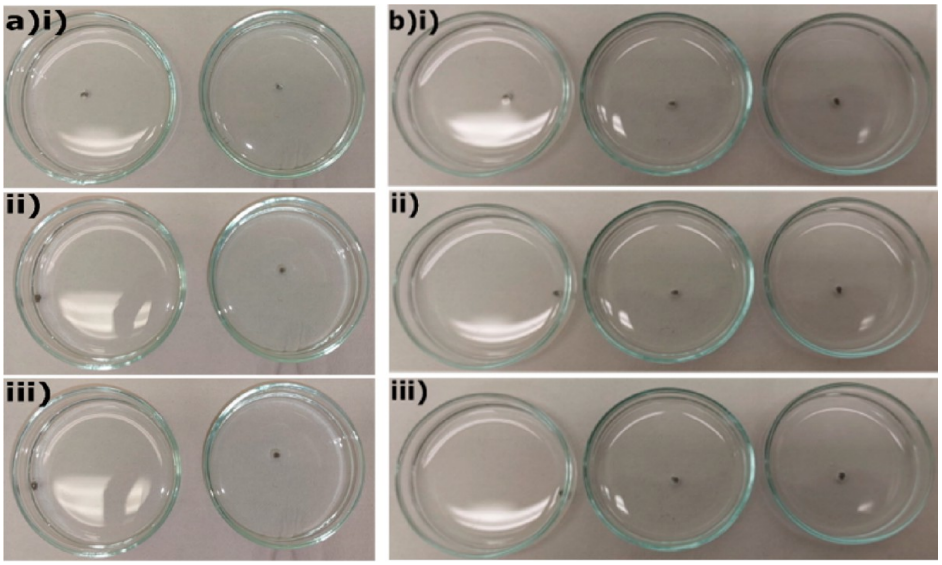

Figure 5. (a) Effect of NaOH treatment shown in captured time frames. (i) At 0 s, as the microengines are introduced to H_2O_2, (ii) at 69 s, as the NaOH-treated microengine reaches the edge of the Petri dish, (iii) at 140 s, even after 140 s, the microengine only treated with sodium hypophosphite does not show any movement. (b) Effect of cavity size at the base shown in captured time frames. (i) At 0 s, as microengines with large, small, and no cavity (from left to right) are introduced to H_2O_2, (ii) at 17 s, as the microengine with a larger cavity at the base reaches the edge of the Petri dish, and (iii) at 140 s, microengines with a smaller and no cavity at the base still do not show any movement.

The observations showed that pretreatment of microengines with NaOH leads to enhanced availability of elemental Pd after the reduction step, as they showed a rapid movement in H_2O_2, while the microengine treated with only sodium hypophosphite showed no movement. This still nature of only the sodium hypophosphite-treated microengine can only be attributed to the washing away of elemental Pd in the wash step, as they are only present on the surface. However, when the microengine is treated with NaOH, it leads to resin ring cleavage, which might lead to the creation of nanopores that entrap ionic Pd, and once the reduction is completed, they become entrapped elemental Pd, which does not wash away in the wash step. Figure 5a illustrates the timeframes for this scenario, while supplementary Video S3 shows the video graphical observation during the experiment.

The microengine treated with NaOH moved at an average velocity of 0.37 mm/s. It is evident that this movement velocity is different from case to case, even though the same treatment conditions or similar experimental conditions were employed. This can be attributed to the discrepancies in manual treatment steps, which could lead to excessive washing that may change the final available Pd concentration. This changes the reaction rate of Pd with H_2O_2, which, in return, changes the movement velocity.

3.2.3. Effect of Cavity Size at the Base. The effect of cavity size at the base of the microengine on movement was also studied. For this, the threaded ovoid microengine was printed with a 1 mm diameter cavity (larger), a 0.2 mm diameter cavity (smaller), and without a cavity (no). The microengines were introduced to H_2O_2 simultaneously, and they were observed for their movement. With time, a rapid movement could be observed for the microengine with a larger cavity at the base. The velocity calculated for this movement was 1.44 mm/s. However, no movement could be observed for the other two microengines, which are smaller and have no cavity at the base.

The larger cavity at the base of the microengine provides an enhanced inner surface area for the microengine in comparison to the other two microengines. This introduces more Pd for the catalytic reaction. Further, with a larger cavity, there is more space for the oxygen bubbles that are formed within the cavity to escape from the cavity, thus giving an additional push to the movement of the microengine. In a smaller cavity, the space is limited, and bubbles might break down within the cavity before they escape through the base. As for the no-cavity microengine, there is no formation of oxygen in an inner cavity, and hence, no additional forces are acting to support the movement. The time frames captured during the observation of movement for this scenario are shown in Figure 5b, and the video file is provided in supplementary Video S4.

3.2.4. Effect of Design. Herein, we studied the design of the microengine as another aspect that affects its movement. Three designs , threaded ovoid, ovoid, and cone, were designed by using SolidWorks software and realized via customized DLP 3D printing. All three designs were equipped with a larger cavity of 1 mm diameter at the base. The weight, volume, and surface area for the threaded ovoid are 6.0 mg, 4.6 mm^3, and 26.78 mm^2. This results in a surface area/volume ratio of 5.82 and a density of 1.3 mg/mm^3. For the ovoid, these values become slightly lower as the thread is no longer there. The values are 5.4 mg, 4.27 mm^3, and 19.97 mm^2, respectively, resulting in a surface area-to-volume ratio of 4.68 and a density of 1.26 mg/mm^3. For the cone design, weight, volume, and area show the lowest values among the three designs, which are 2.2 mg, 1.83 mm^3, and 14.75 mm^2, respectively, resulting in a density of 1.20 mg/mm^3. However, the surface area to volume ratio of the cone design is reported to be the highest among the three designs, at 8.06.

Upon experimentation, we observed the fastest movement with threaded ovoid, followed by cone and then by ovoid. The reported average velocities are 1.86, 0.77, and 0.42 mm/s for threaded ovoid, cone, and ovoid, respectively. The rapid movement of the threaded ovoid can be attributed to the additional surface area offered by the thread and the restriction it provides in the direction of bubble release. Additional surface area offers more active sites to carry out the catalytic reaction,

https://doi.org/10.1021/acsomega.3c04949
ACS Omega 2024, 9, 283−293

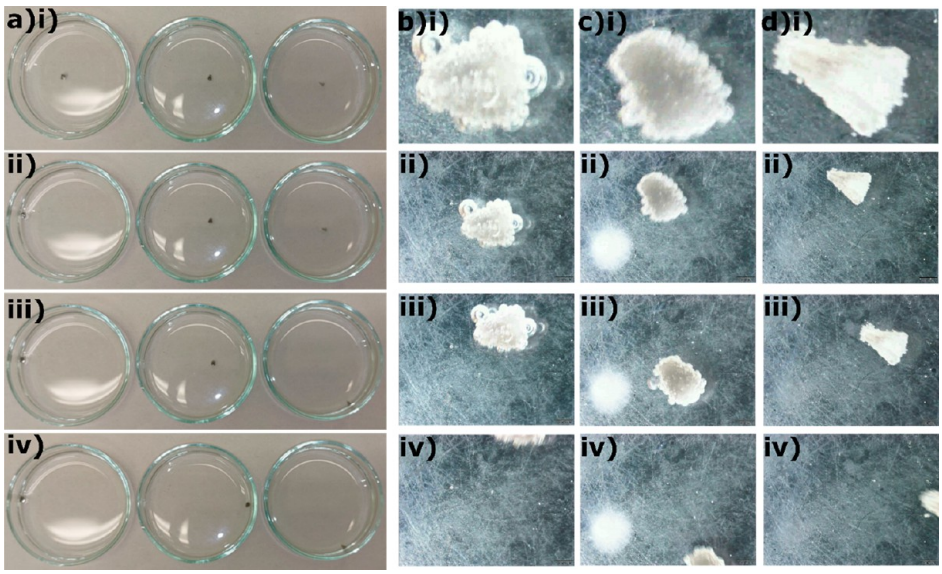

Figure 6. (a) Movement, as observed for the threaded ovoid, ovoid, and cone design (from left to right, respectively) microengines in H_2O_2. (i) At the beginning of introduction of microengines, (ii) at 13 s as the threaded ovoid reaches the edge of the Petri dish, (iii) at 35 s as the cone reaches the edge of the Petri dish, and (iv) at 53 s as the ovoid reaches the edge of the Petri dish. (b) Bubbling and movement observed for threaded ovoids under a microscope. (i) Excessive bubbling observed due to thread and (ii−iv) movement of the threaded ovoid within 2.4 s (to exit the captured area under the microscope). (c) Bubbling and movement observed for the ovoid under a microscope. (i) Bubbling is not excessive and is spreaded and (ii−iv) movement of the ovoid within 3.3 s. (d) Bubbling and movement observed for the cone under a microscope. (i) Bubbling density is larger at the tip and (ii−iv) movement of the threaded ovoid within 2.8 s.

while directional bubble release increases the driving force in a certain direction. Also, the threaded design may induce an effect on movement against the surface tension of the medium due to its extruded nature. As for the cone, although the surface area is the lowest, its surface area to volume is the highest, and this may support the microengine to move faster when compared to the ovoid. Also, the cone design itself has a positive effect on moving against the surface tension of the media. However, the design shows a lower velocity than the threaded ovoid, as it has a lower surface area. In the ovoid design, it is obvious that it does not possess the advantages of an additional surface area, restricted directional movement of bubble release, and extrusions to support movement against the surface tension of the media, as this design does not have a thread. Hence, the design shows the lowest velocity of all three. The time frames captured during the movement are provided in Figure 6a, while the bubbling effect observed under the microscope is provided in Figure 6b−d with the movement captured under the microscope. Figure 6b clearly shows that the tread helps in the enhancement of bubbling and creates a directional bubbling effect, whereas without a thread, bubbling is limited, and the bubbles are released from all sides of the surface, according to Figure 6c. Figure 6d illustrates that for the cone design as well, bubbling is enhanced at the tip of the cone, and the bubbling density is larger there, guiding the movement in the opposite direction. The movement of these designs in H_2O_2 is provided in supplementary Video S5, while supplementary Videos S6, S7, and S8 provides the trajectory of movement observed under the microscope for threaded ovoid, ovoid, and cone, respectively.

Figure 7 illustrates the trajectory of movement for the threaded ovoid, ovoid, and cone in detail. The time frames captured here are respective to supplementary Videos S6, S7, and S8 and are different from Figure 6b−d, which were captured from different runs for each design. The observations further show that even for the same design, the direction of movement and speed could differ depending on the distribution of the catalyst and the degree of treatment, as we discussed in an earlier section.

3.2.5. Effect of the Active Surface Area. To understand the effect of surface area, we covered the outer surface of threaded ovoid with resin and observed its movement in H_2O_2 in comparison to the threaded ovoid microengine without surface coverage. To cover the outer surface, we dipped the threaded ovoid head down in a thin layer of PMMA-like resin. Then, it was taken out immediately and cured under UV light. This leads to a slight increase of weight of the microengine as well. As a result, only the inner surface of the cavity is left to support the bubbling reaction, as only the inner cavity is composed of catalyst resin.

The results show that the inner surface area is not sufficient to provide a driving force for the movement of microengines in this case, where the engines are printed with 3D printing on a smaller scale. The microengine that was not covered showed movement with an average velocity of 0.75 mm/s in this case, while the surface-covered microengine showed no movement. This could be affected by the surface cover that introduces a blunt surface without extrusions to the microengine. The smooth nature of the surface hinders the microengine's action against the surface tension of H_2O_2. Hence, in such a scenario, a larger driving force is required, and the inner surface area alone is not sufficient to provide the required driving force. To further study this scenario, we recommend the employment of selective printing of microengines without affecting the surface morphology of the microengine. The effect is illustrated in Figure 8a (supplementary Video S9) with captured time frames during recording of the movement.

3.2.6. Effect of Pd Concentration. Another critical factor that affects the locomotion of the microengine is the Pd concentration in catalyst resin. To investigate this effect, we reduced the Pd concentration from 700 to 350 ppm in one set of

https://doi.org/10.1021/acsomega.3c04949
ACS Omega 2024, 9, 283−293

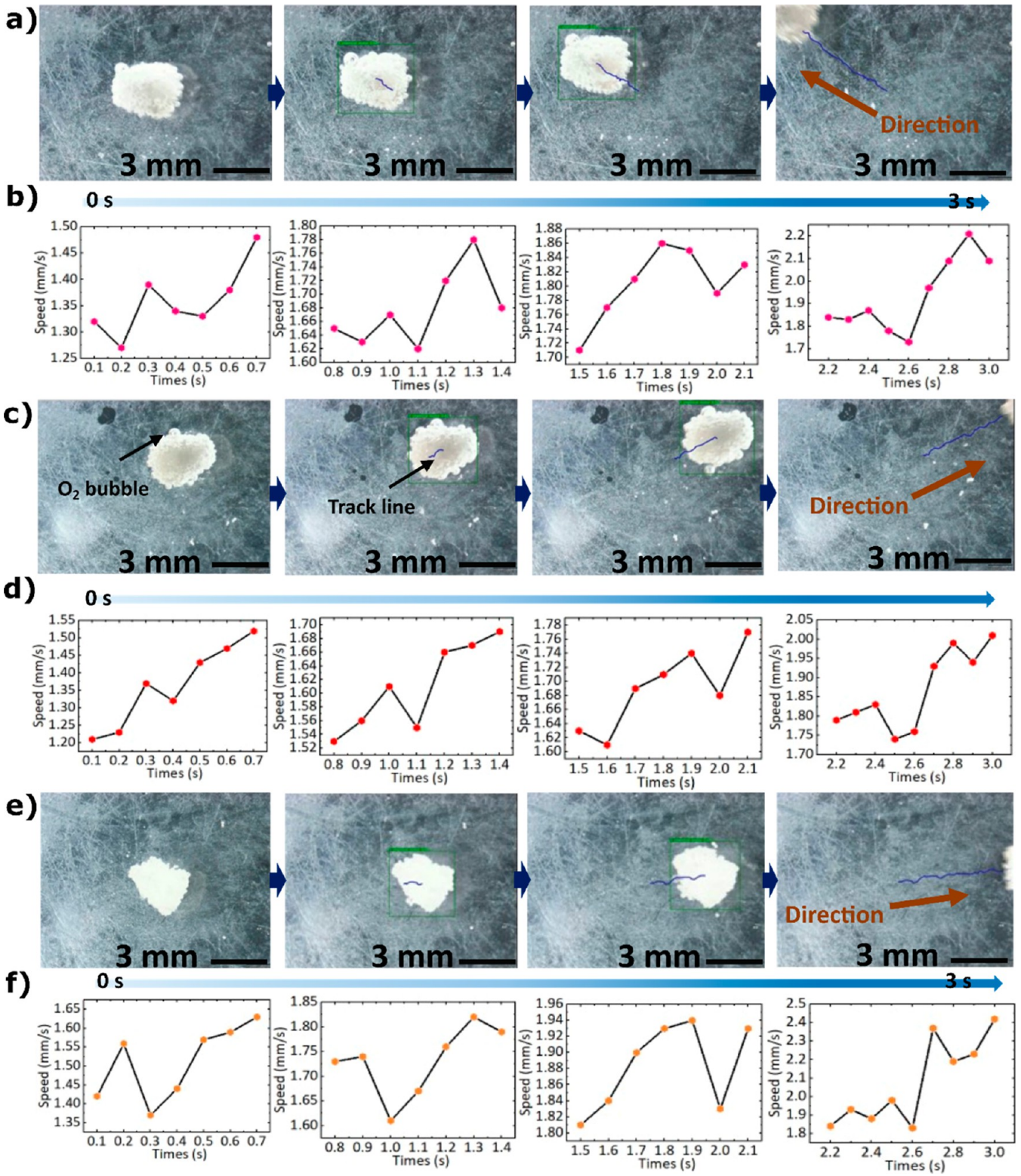

Figure 7. Figurative and graphical illustration for the movement trajectory and speed of threaded ovoid, ovoid, and cone designs. (a) Trajectory for movement of the threaded ovoid with (b) speed over time. (c) Trajectory for movement of the ovoid with (d) speed over time. (e) Trajectory for movement of the cone with (f) speed over time.

threaded ovoid microengines. The catalyst resin was prepared accordingly, and printing was performed.

Upon subjecting them to the experiment to observe their movement in H_2O_2, no movement could be observed. Yet, bubbling was observed to a certain extent, which was not rigorous. The observation is provided in Figure 8b, where Figure 8b(i) demonstrates the bubbling observed under the microscope and Figure 8b(ii−v) demonstrates that no movement is observed over time (supplementary Video S10). The result can be attributed to the lower concentration of Pd present in the

https://doi.org/10.1021/acsomega.3c04949
ACS Omega 2024, 9, 283−293

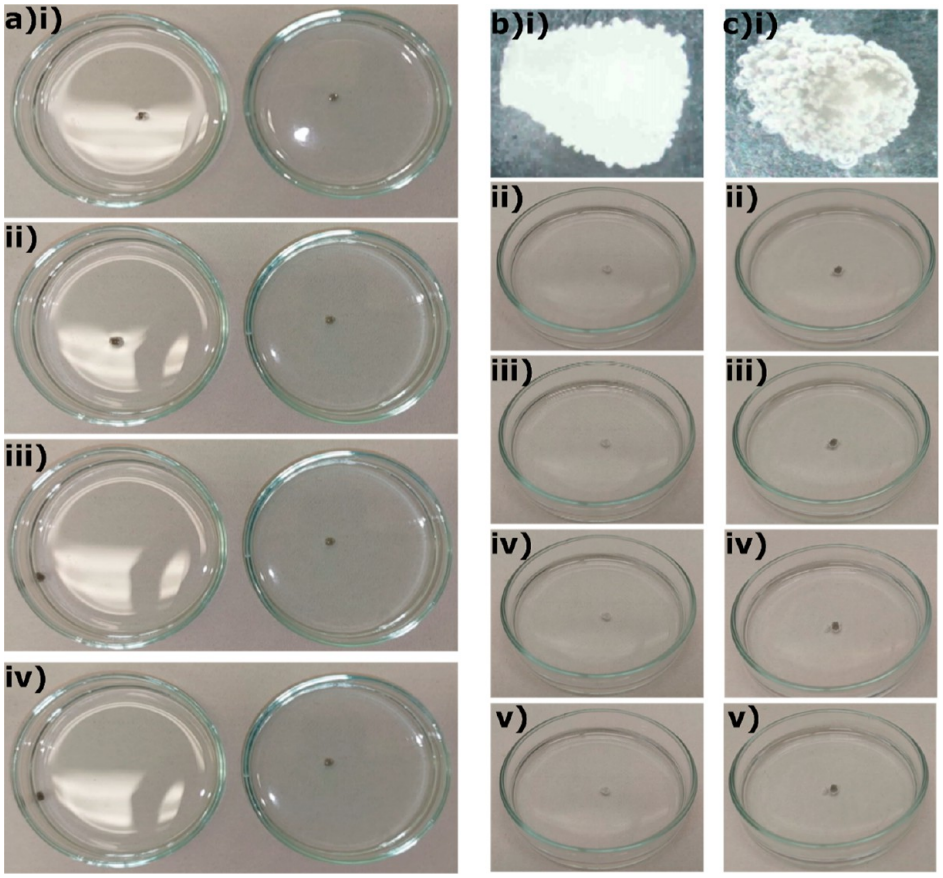

Figure 8. (a) Effect of the active surface area on the movement of microengines shown with surface uncovered (left) and surface covered (right) threaded ovoid microengines. (i) At 0 s, as microengines are introduced to H_2O_2, (ii) at 32 s, uncovered microengine has moved slightly while the covered microengine remains stagnant, (iii) at 45 s, the uncovered microengine reaches the edge of the Petri dish and the covered microengine still remains stagnant, and (iv) after 72 s, the covered microengine still remains stagnant, showing no movement. (b) Effect of Pd concentration shown with a microengine printed using catalyst resin containing 350 ppm of Pd. (i) Catalytic reaction is present on the microengine surface, producing oxygen bubbles, (ii) at 0 s, as the microengine is introduced to the H_2O_2, (iii) at 48 s, no displacement has occurred from the original position, (iv) at 96 s, the microengine remains stagnant, (v) after 145 s, the microengine still remains stagnant. (c) Effect of H_2O_2 concentration on the locomotion of a microengine illustrated with a threaded ovoid microengine in 15% (w/w) H_2O_2. (i) Bubbling or the catalytic reaction occurs even at a lowered H_2O_2 concentration, (ii) at 0 s, as the microengine is introduced to 15% H_2O_2, and (iii) at 64 s to (iv) 66 s, a rapid rotation movement is observed, and the microengine moves slightly from its original position. In (iv), the original position can be seen as a patch of bubbles to the left of the microengine; (v) after 145 s, no movement is observed after the slight movement occurred at 64 s, and the microengine remains in the position it obtained during rotation.

microengine for the catalytic reaction to create an ample driving force for the locomotion of the microengine. Herein, it should be noted that, while the catalyst resin is being prepared, the catalyst is mixed with resin, and thus the Pd concentration implies the total Pd concentration available within the resin. A certain portion of this Pd might as well remain within the microengine without being able to participate in the reaction. Hence, the Pd available for the reaction goes further down. In this scenario, where the Pd concentration is halved from the original concentration of 700 ppm, this effect becomes significant, and in return, the locomotion of the microengine is not observed, even though the catalytic reaction is present on the surface of the microengine in the form of bubbling.

3.2.7. Effect of H_2O_2 Concentration. Once the factors related to the microengine, such as design, cavity size, and Pd concentration, were studied, we studied the effect of H_2O_2 concentration in the media on the locomotion of microengines. In an earlier section, Section 3.2.1, we showed that H_2O_2 is necessary for the catalytic reaction as the catalytic Pd reacts with H_2O_2 to produce oxygen, which provides the driving force for the locomotion of microengines. In this section, we study the effect of H_2O_2 concentration by lowering it to 15% (w/w) from the original concentration of 30% (w/w) used in all the other experiments except for the experiment where water is used as the medium. Here, we used a threaded ovoid microengine with a larger cavity at the base printed with 700 ppm Pd catalyst resin for the experiment.

Since the beginning of the introduction of the microengine to 15% (w/w) H_2O_2, no movement has been observed until 64 s. Yet, we observed that a catalytic reaction is occurring on the surface of the microengine. From 64 to 66 s, the microengine rotates as a result of a catalytic reaction and changes its original position slightly. This implies that the 15% (w/w) H_2O_2 concentration is capable of providing a slight rotational movement to the smaller-scale microengine as the oxygen bubbles are stacked up to a certain limit. However, the microengine remained motionless there even after 145 s. Hence, it can be concluded that a 15% (w/w) H_2O_2 concentration is insufficient to obtain continuous motion from a microengine. Figure 8c demonstrates this phenomenon

https://doi.org/10.1021/acsomega.3c04949
ACS Omega 2024, 9, 283−293

figuratively with the bubbling reaction observed under a microscope Figure 8c(i) and time frames captured during the study of movement Figure 8c(ii–v). Supplementary Video S11 shows the still nature of the microengine in 15% (w/w) H_2O_2.

4. CONCLUSIONS

Here, we report a simple, rapid, inexpensive, and easily modifiable single-step method for the realization of self-propelling microengines via 3D printing of microengines utilizing a catalyst resin. We demonstrate the self-propelled movement of such printed microengines of three different designs, such as threaded ovoid, ovoid, and cone, in which the overall volumes do not exceed 5 mm^3. H_2O_2 is used as the fuel, and the microengines were studied for their design, internal cavity size at the base, active surface area, pretreatment conditions, Pd concentration, role of H_2O_2, and concentration of H_2O_2 as to how these factors affect the self-propelled locomotion of the microengines. The current study does not focus on the magnetic manipulation of motion of microengines since the characterization of previously mentioned parameters for self-propulsion of 3D-printed microengines was the major purpose of the study. The obtained results indicate that a threaded ovoid design with a larger cavity of 1 mm diameter at the base stands out from the rest of the design in terms of the speed of the motion. Also, it was evident that a larger cavity size supports movement by providing more space to escape for oxygen produced on the inner surface. We observed that a 700 ppm concentration of Pd in catalyst resin in a 30% (w/w) H_2O_2 medium works best among the studied conditions. Finally, we have demonstrated that this modified catalyst resin 3D printing enables the realization of microengines that can be optimized and modified to be suitable for numerous applications through the modification of catalyst and other additives to the resin and the type of fuel. The developed method could stand out from the complicated, time-consuming methods as it is a simple, rapid, and inexpensive single-step process.

■ ASSOCIATED CONTENT

Supporting Information

The Supporting Information is available free of charge at https://pubs.acs.org/doi/10.1021/acsomega.3c04949.

List of video files (PDF)
Movement in water (AVI)
Movement in Hydrogen Peroxide (AVI)
Effect of NaOH treatment (AVI)
Effect of cavity size at the base (AVI)
Effect of design (AVI)
Threaded ovoid_Movement trajectory (AVI)
Ovoid_Movement trajectory (AVI)
Cone_Movement trajectory (AVI)
Effect of active surface area (AVI)
Effect of Pd concentration (AVI)
Effect of hydrogen peroxide concentration (AVI)

■ AUTHOR INFORMATION

Corresponding Authors

Shinjiro Umezu − *Graduate School of Creative Science and Engineering, Department of Modern Mechanical Engineering, Waseda University, Tokyo 169-8555, Japan;* orcid.org/0000-0003-2146-5344; Email: umeshin@waseda.jp

Hirotaka Sato − *School of Mechanical and Aerospace Engineering, Nanyang Technological University, Singapore 637460, Singapore;* orcid.org/0000-0003-4634-1639; Email: hirosato@ntu.edu.sg

Authors

Adhikarige Taniya Kaushalya Perera − *School of Mechanical and Aerospace Engineering, Nanyang Technological University, Singapore 637460, Singapore*

Kewei Song − *Graduate School of Creative Science and Engineering, Department of Modern Mechanical Engineering, Waseda University, Tokyo 169-8555, Japan*

Xiangyi Meng − *Graduate School of Creative Science and Engineering, Department of Modern Mechanical Engineering, Waseda University, Tokyo 169-8555, Japan*

Wei Yang Wan − *School of Mechanical and Aerospace Engineering, Nanyang Technological University, Singapore 637460, Singapore*

Complete contact information is available at: https://pubs.acs.org/10.1021/acsomega.3c04949

Author Contributions

A.T.K.P. and K.S. equally contributed to this work. **Adhikarige Taniya Kaushalya Perera:** methodology, investigation, writing—original draft, writing—review and editing, visualization, and data curation; **Kewei Song:** methodology, investigation, and writing—review and editing; **Xiangyi Meng:** data curation; **Wan Wei Yang:** data curation; **Shinjiro Umezu:** conceptualization, methodology, investigation, supervision, project administration, and funding acquisition; **Hirotaka Sato:** conceptualization, methodology, investigation, writing—original draft, writing—review and editing, visualization, supervision, project administration, and funding acquisition.

Notes

The authors declare no competing financial interest.

■ ACKNOWLEDGMENTS

The authors would like to thank Koh Joo Luang (Nanyang Technological University, NTU), Shinji Nishimura, and Seiko Itagaki (Waseda University) for their support in facilitating and maintaining the research environment, and also Kunlin Wu and Prof. Yifan Wang (NTU) for their technical support and discussion. This work was supported by the Singapore Ministry of Education [RG140/20], NTUitive Pte Ltd [NGF-2022-11-020], JST SPRING (grant number JPMJSP2128), JST-Mirai Program (grant number JPMJMI21I1), and KAKENHI (grant numbers 19H02117 and 20K20986), Japan, and Frontier of Embodiment Informatics: ICT and Robotics, under Waseda University's Waseda Goes Global Plan, as part of The Japanese Ministry of Education, Culture, Sports, Science and Technology (MEXT)'s Top Global University Project.

■ REFERENCES

(1) Wang, H.; Zhao, G.; Pumera, M. Crucial role of surfactants in bubble-propelled microengines. *J. Phys. Chem. C* **2014**, *118* (10), 5268−5274.

(2) Huang, G.; Wang, J.; Mei, Y. Material considerations and locomotive capability in catalytic tubular microengines. *J. Mater. Chem.* **2012**, *22* (14), 6519−6525.

(3) Manesh, K. M.; Cardona, M.; Yuan, R.; Clark, M.; Kagan, D.; Balasubramanian, S.; Wang, J. Template-assisted fabrication of salt-independent catalytic tubular microengines. *ACS Nano* **2010**, *4* (4), 1799−1804.

(4) He, Y.; Wu, J.; Zhao, Y. Designing catalytic nanomotors by dynamic shadowing growth. *Nano Lett.* **2007**, *7* (5), 1369−1375.

(5) Paxton, W. F.; Sundararajan, S.; Mallouk, T. E.; Sen, A. Chemical locomotion. *Angew. Chem., Int. Ed.* **2006**, *45* (33), 5420−5429.
(6) Solovev, A. A.; Mei, Y.; Bermúdez Ureña, E.; Huang, G.; Schmidt, O. G. Catalytic microtubular jet engines self-propelled by accumulated gas bubbles. *Small* **2009**, *5* (14), 1688−1692.
(7) Orozco, J.; García-Gradilla, V.; D'Agostino, M.; Gao, W.; Cortés, A.; Wang, J. Artificial enzyme-powered microfish for water-quality testing. *ACS Nano* **2013**, *7* (1), 818−824.
(8) Patra, D.; Sengupta, S.; Duan, W.; Zhang, H.; Pavlick, R.; Sen, A. Intelligent, self-powered, drug delivery systems. *Nanoscale* **2013**, *5* (4), 1273−1283.
(9) Burdick, J.; Laocharoensuk, R.; Wheat, P. M.; Posner, J. D.; Wang, J. Synthetic nanomotors in microchannel networks: Directional microchip motion and controlled manipulation of cargo. *J. Am. Chem. Soc.* **2008**, *130* (26), 8164−8165.
(10) Gao, W.; Sattayasamitsathit, S.; Uygun, A.; Pei, A.; Ponedal, A.; Wang, J. Polymer-based tubular microbots: role of composition and preparation. *Nanoscale* **2012**, *4* (7), 2447−2453.
(11) Ebbens, S. J.; Howse, J. R. In pursuit of propulsion at the nanoscale. *Soft Matter* **2010**, *6* (4), 726−738.
(12) Paxton, W. F.; Kistler, K. C.; Olmeda, C. C.; Sen, A.; Angelo, S. K.; Cao, Y.; Mallouk, T. E.; Lammert, P. E.; Crespi, V. H. Catalytic nanomotors: autonomous movement of striped nanorods. *J. Am. Chem. Soc.* **2004**, *126* (41), 13424−13431.
(13) Mirzazadeh Khomambazari, S.; Yusuf, M.; Esmaeilkhanian, A.; Zarei, R.; Hojjati, M.; Sharifianjazi, F.; Arabuli, L. Review of bubble and magnetically driven catalytic micro/nanomotors: Fabrication and characterization. *J. Compos. Compd.* **2022**, *4* (13), 220−231.
(14) Naeem, S.; Naeem, F.; Mujtaba, J.; Shukla, A.; Mitra, S.; Huang, G.; Gulina, L.; Rudakovskaya, P.; Cui, J.; Tolstoy, V.; et al. Oxygen generation using catalytic nano/micromotors. *Micromachines* **2021**, *12* (10), 1251.
(15) Londhe, V.; Sharma, P. Unfolding the future: Self-controlled catalytic nanomotor in healthcare system. *Mater. Sci. Eng., C* **2020**, *117*, 111330.
(16) Ismagilov, R. F.; Schwartz, A.; Bowden, N.; Whitesides, G. M. Autonomous movement and self-assembly. *Angew. Chem., Int. Ed.* **2002**, *41* (4), 652−654.
(17) Gao, W.; Sattayasamitsathit, S.; Wang, J. Catalytically propelled micro-/nanomotors: how fast can they move? *Chem. Rec.* **2012**, *12* (1), 224−231.
(18) Wang, H.; Zhao, G.; Pumera, M. Beyond platinum: Bubble-propelled micromotors based on Ag and MnO2 catalysts. *J. Am. Chem. Soc.* **2014**, *136* (7), 2719−2722.
(19) Gao, W.; Dong, R.; Thamphiwatana, S.; Li, J.; Gao, W.; Zhang, L.; Wang, J. Artificial micromotors in the mouse's stomach: A step toward in vivo use of synthetic motors. *ACS Nano* **2015**, *9* (1), 117−123.
(20) Gao, W.; Uygun, A.; Wang, J. Hydrogen-bubble-propelled zinc-based microrockets in strongly acidic media. *J. Am. Chem. Soc.* **2012**, *134* (2), 897−900.
(21) Gao, W.; Pei, A.; Wang, J. Water-driven micromotors. *ACS Nano* **2012**, *6* (9), 8432−8438.
(22) Gao, W.; Feng, X.; Pei, A.; Gu, Y.; Li, J.; Wang, J. Seawater-driven magnesium based Janus micromotors for environmental remediation. *Nanoscale* **2013**, *5* (11), 4696−4700.
(23) Mou, F.; Chen, C.; Ma, H.; Yin, Y.; Wu, Q.; Guan, J. Self-propelled micromotors driven by the magnesium−water reaction and their hemolytic properties. *Angew. Chem., Int. Ed.* **2013**, *52* (28), 7208−7212.
(24) Li, J.; Singh, V. V.; Sattayasamitsathit, S.; Orozco, J.; Kaufmann, K.; Dong, R.; Gao, W.; Jurado-Sanchez, B.; Fedorak, Y.; Wang, J. Water-driven micromotors for rapid photocatalytic degradation of biological and chemical warfare agents. *ACS Nano* **2014**, *8* (11), 11118−11125.
(25) Zhu, W.; Li, J.; Leong, Y. J.; Rozen, I.; Qu, X.; Dong, R.; Wu, Z.; Gao, W.; Chung, P. H.; Wang, J.; et al. 3D-Printed Artificial Microfish. *Adv. Mater.* **2015**, *27* (30), 4411−4417.
(26) Tan, Y.; Gu, J.; Zang, X.; Xu, W.; Shi, K.; Xu, L.; Zhang, D. Versatile Fabrication of Intact Three-Dimensional Metallic Butterfly Wing Scales with Hierarchical Sub-micrometer Structures. *Angew. Chem., Int. Ed.* **2011**, *50* (36), 8307−8311.
(27) Liu, K.; Yang, Q.; Zhao, Y.; Chen, F.; Shan, C.; He, S.; Fan, X.; li, L.; Meng, X.; Du, G.; et al. Three-dimensional metallic micro-components achieved in fused silica by a femtosecond-laser-based microsolidifying process. *Microelectron. Eng.* **2014**, *113*, 93−97.
(28) Zhan, J.; Tamura, T.; Li, X.; Ma, Z.; Sone, M.; Yoshino, M.; Umezu, S.; Sato, H. Metal-plastic hybrid 3D printing using catalyst-loaded filament and electroless plating. *Addit. Manuf.* **2020**, *36*, 101556.
(29) Song, K.; et al. New metal-plastic hybrid additive manufacturing strategy: Fabrication of arbitrary metal-patterns on external and even internal surfaces of 3D plastic structures. **2021** arXiv:2112.11661, arXiv preprint.
(30) Perera, A.; Wu, K.; Wan, W. Y.; Song, K.; Meng, X.; Umezu, S.; Wang, Y.; Sato, H. Modified polymer 3D printing enables the formation of functionalized micro-metallic architectures. *Addit. Manuf.* **2023**, *61*, 103317.
(31) Xu, C.; Yang, Z.; Lum, G. Z. Small-Scale Magnetic Actuators with Optimal Six Degrees-of-Freedom. *Adv. Mater.* **2021**, *33* (23), 2100170.
(32) Xu, C.; Yang, Z.; Tan, S. W. K.; Li, J.; Lum, G. Z. Magnetic Miniature Actuators with Six-Degrees-of-Freedom Multimodal Soft-Bodied Locomotion. *Adv. Intell. Syst.* **2022**, *4* (4), 2100259.
(33) Li, M.; Xia, Z.; Luo, M.; He, L.; Tao, L.; Yang, W.; Yu, Y.; Guo, S. Structural Regulation of Pd-Based Nanoalloys for Advanced Electrocatalysis. *Small Sci.* **2021**, *1* (11), 2100061.
(34) Grigoriev, S.; Lyutikova, E.; Martemianov, S.; Fateev, V. On the possibility of replacement of Pt by Pd in a hydrogen electrode of PEM fuel cells. *Int. J. Hydrogen Energy* **2007**, *32* (17), 4438−4442.
(35) Wang, X.; Li, Z.; Qu, Y.; Yuan, T.; Wang, W.; Wu, Y.; Li, Y. Review of Metal Catalysts for Oxygen Reduction Reaction: From Nanoscale Engineering to Atomic Design. *Chem* **2019**, *5* (6), 1486−1511.
(36) Chen, L.; Medlin, J. W.; Grönbeck, H. On the Reaction Mechanism of Direct H2O2 Formation over Pd Catalysts. *ACS Catal.* **2021**, *11* (5), 2735−2745.
(37) Bente, K.; Codutti, A.; Bachmann, F.; Faivre, D. Biohybrid and Bioinspired Magnetic Microswimmers. *Small* **2018**, *14* (29), 1704374.
(38) Kósa, G.; Jakab, P.; Székely, G.; Hata, N. MRI driven magnetic microswimmers. *Biomed. Microdevices* **2012**, *14*, 165−178.
(39) Xie, L.; Pang, X.; Yan, X.; Dai, Q.; Lin, H.; Ye, J.; Cheng, Y.; Zhao, Q.; Ma, X.; Zhang, X.; et al. Photoacoustic imaging-trackable magnetic microswimmers for pathogenic bacterial infection treatment. *ACS Nano* **2020**, *14* (3), 2880−2893.
(40) Kadry, H.; Wadnap, S.; Xu, C.; Ahsan, F. Digital light processing (DLP) 3D-printing technology and photoreactive polymers in fabrication of modified-release tablets. *Eur. J. Pharm. Sci.* **2019**, *135*, 60−67.

https://doi.org/10.1021/acsomega.3c04949
ACS Omega 2024, 9, 283−293